

# Chapter 10

## Computational Modelling on Lithium-Ion Battery Pack Forced Convection Cooling



**Prakash Ghose, Swarup Kumar Nayak, Basanta Kumar Rana,  
and Jitendra Kumar Patel**

**Abstract** Lithium-ion batteries are widely used in cell phones, laptops and battery vehicles. However, during discharge, a huge amount of heat is generated in the cell core. Thermal management of the battery pack is much important, particularly for electric vehicles to reduce fire hazards. In this work, CFD simulations are performed to evaluate the cooling effect of a  $4 \times 4$  Lithium-ion battery pack with different discharge rates and different airflow velocities. From the results it is observed that cells present downstream have a higher temperature as compared to the cells placed upstream irrespective of discharge rate and airflow rate. The two mid-cells in the last row have the highest temperature in any operating condition. When the discharge rate increases, the amount of heat generation in the cells increases. Hence, the temperature of the corresponding cell in each row is relatively higher as compared to the low discharge rate condition. Similarly, with an increase in airflow velocity, the cooling rate of the battery pack is enhanced.

### 10.1 Introduction

Hydrocarbon fuel-driven automobiles are one of the major sources of air pollution.  $\text{CO}_2$ , CO,  $\text{NO}_x$  emissions from automobiles affect human health and are also responsible for global warming. Today electric vehicles are the most prominent alternative to fuel-driven vehicles. Though electric vehicle technology is not a new concept but due to the poor energy storage capacity of lead-acid and Nickel–cadmium batteries, electric vehicles were not popular. Lithium-Ion battery technology now changed the scenario of electric vehicles due to its high energy storage ability. However, during charging and particularly during discharging, a huge amount of heat is generated from the Li-Ion battery. Therefore, the thermal management of the battery is an

---

P. Ghose (✉) · S. K. Nayak · B. K. Rana · J. K. Patel  
School of Mechanical Engineering, KIIT Deemed to be University, Bhubaneswar 751024, India  
e-mail: [pghosefme@kiit.ac.in](mailto:pghosefme@kiit.ac.in)

© The Author(s), under exclusive license to Springer Nature Singapore Pte Ltd. 2024  
P. H. V. S. Talpa Sai et al. (eds.), *Intelligent Manufacturing and Energy Sustainability*,  
Smart Innovation, Systems and Technologies 372,  
[https://doi.org/10.1007/978-981-99-6774-2\\_10](https://doi.org/10.1007/978-981-99-6774-2_10)

105

important factor hence cooling system should be designed properly. Otherwise, fire hazards may cause a severe accidents.

Wang et al. [1] investigated battery cooling through forced convection with various cell arrangement structures. It has been reported that a fan placed on the top of the module is the best cooling method. A cubic arrangement of cells is a better option for cooling and also it is cost-effective. On the other hand, hexagonal cell arrangement is best as space utilization is a concern. In another work, Wang et al. [2] conducted CFD simulations to investigate the temperature distribution and heat transfer of Lithium-Ion batteries through air cooling. It is suggested that if the ambient temperature is below 20 °C, forced convection for cooling is not required. Also, it is mentioned that the upper ambient temperature limit is 35 °C with forced convection cooling. Saw et al. [3] developed new correlations for the Nusselt number and Reynolds number from their experimental and CFD study, where the air is used as a cooling fluid. Xu et al. [4, 5] used U-shaped duct and baffle plates respectively to enhance the battery cooling using air as working fluid. Many researchers also used heat pipes to improve the heat transfer rate on battery cooling [6–8]. Battery cooling using phase change material is also a method [9, 10] that is investigated by many researchers. Hybrid cooling processes such as; (i) PCM is used as a primary coolant and water is used as a secondary coolant (ii) PCM used in heat pipe etc. are also investigated for cooling enhancement [11, 12]. To increase the cooling effect, Ethyl glycol–water,  $\text{Al}_2\text{O}_3$ -water,  $\text{ZnO}$ -water and  $\text{CuO}_2$ -water nanofluids are also used for battery cooling and performance has been investigated [13, 14].

In the current simulation, a  $4 \times 4$  lithium-Ion battery pack is used for simulation to investigate the cooling effect of the battery pack with different battery discharge rates and airflow velocities are acceptable.

## 10.2 Methodology

A  $4 \times 4$  lithium-Ion battery pack is used for simulation as shown in Fig. 10.1. The gap between two consecutive cells in the lateral direction is 3 mm and the gap between two consecutive cells in the longitudinal direction is 6 mm. The height of the cell is 90 mm and the diameter of the lithium-ion core is 18 mm and it is covered with a 1.5 mm thick steel casing. The battery pack cover dimension is 91 mm  $\times$  82 mm  $\times$  100 mm.

The computational geometry has three domains such as; (i) Fluid domain (ii) Lithium-ion core and an (iii) Steel cover. The geometry is prepared with the help of Ansys Design modeler and meshed using Ansys Meshing tool. The entire domain has meshed with 1.5 million hexahedra cells. The interfaces between the overlapping domains are converted to the coupled boundary so that only heat exchanges between the domains will be possible. One face of the fluid domain along the longitudinal direction is given as the inlet boundary and the opposite plane is kept as the outlet boundary. The remaining faces of the fluid domain are the adiabatic boundaries.

**Fig. 10.1** Lithium-ion battery pack geometrical configuration

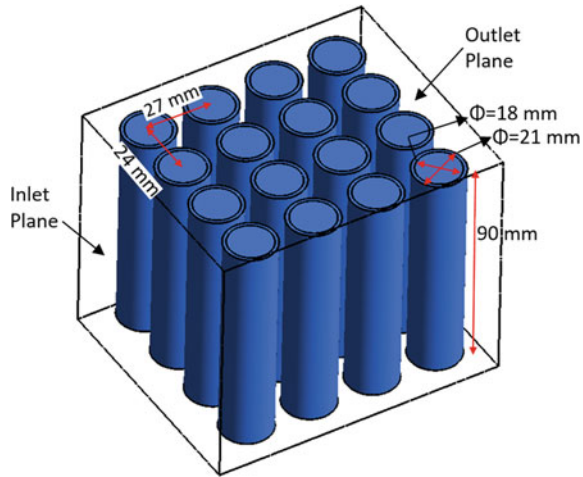


**Table 10.1** Properties of lithium-ion cell [15]

Property	Values
Rated voltage	3.2 V
Rated current	1.35 Ah
Density	2018 kg/m <sup>3</sup>
Specific heat	1282 J/kg K
Volume	0.0000227 m <sup>3</sup>
Thermal conductivity	Radial: 0.9 W/mK Axial: 2.7 W/mK

In this simulation, a 18,650 battery is used. The physical properties of the battery core are given in Table 10.1.

Orthogonal conductivity is used for the Lithium-ion core. The standard constant thermophysical properties of steel are used for the battery cover. Also, the standard constant thermophysical properties of air are used for the fluid domain. Buoyancy-driven heat transfer is not considered in this work. Only force convection cooling is considered. Continuous cooling is required for the battery as heat generates during battery discharge. The heat generation theory proposed by Bernadi [16] is used as given in Eq. (10.1).

$$Q_g = \frac{1}{V_{battery}} \left[ i^2 R_i + iT \frac{dU_0}{dT} \right] \tag{10.1}$$

The first parameter in the bracket of Eq. (10.1) is the polarization heating effect and the second term is the Joule heating effect.  $V_{battery}$  is the battery volume,  $i$  is the current flow during discharge,  $R_i$  is the internal resistance,  $T$  is the battery temperature and the term  $\frac{dU_0}{dT}$  is the parameter which is related to an electrochemical

**Table 10.2** Operating conditions

Cases	Discharge rate	Current (A)	Heat rate (W/m <sup>3</sup> )	Airflow velocity (m/s)
1	1C (discharge in 1 h)	1.35	5318	0.01
2	2C (discharge in 30 min)	2.07	19,452	0.01
3	2C (discharge in 30 min)	2.07	19,452	0.1

reaction. In this work, the internal resistance is set as  $0.04 \Omega$  and the term  $T \frac{dU_0}{dT}$  is taken as  $0.01116 \times$  rated voltage [15].

Simulations are conducted for two discharging conditions where the air flow rate is kept as  $0.01 \text{ m/s}$ . Simulations are also performed with different air flow rates where the discharge rate is kept constant. The cases simulated are given in Table 10.2.

Steady-state mass, momentum and energy conservation equations in Reynolds averaged form are solved along with  $k$  and  $\epsilon$  equations of the standard  $k$ - $\epsilon$  model. The heat rate values given in Table 10.2 are set as a constant source of the lithium-ion core. SIMPLE velocity–pressure coupling approach and second-order upwind spatial discretization scheme are used. Convergence criteria  $10^{-4}$  is set for all governing equations except the energy equation. For the energy equation, it is set as  $10^{-6}$ .

## 10.3 Results and Discussion

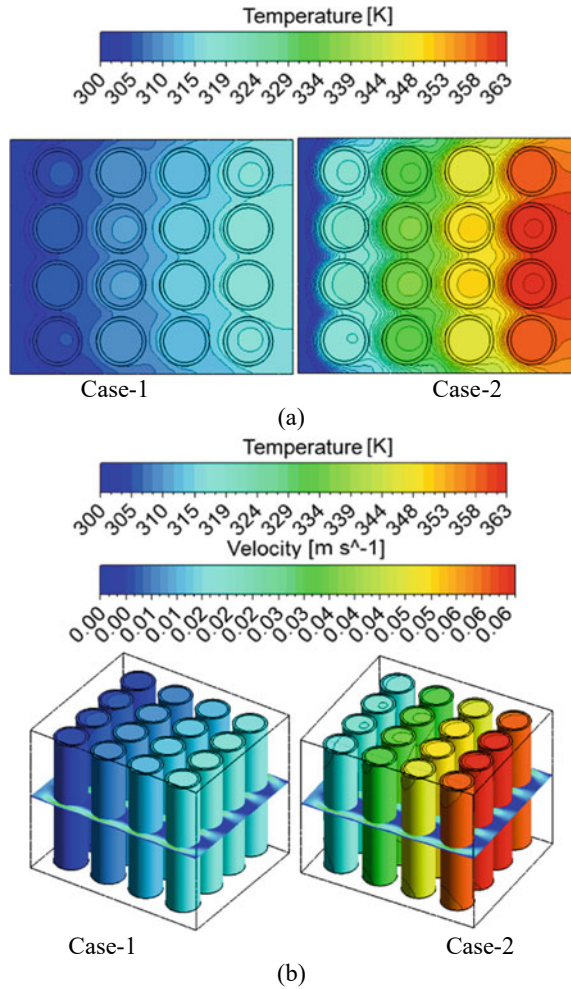
### 10.3.1 Effect of Battery Discharge Rate

Figure 2a shows the temperature distribution across the mid-horizontal plane for case-1 and case-2. Figure 2c shows the 3-D view of the cell cover temperature distribution and the air velocity pattern on the mid-plane for case-1 and case-2.

From both figures, it is observed that in case-1 (1C discharge rate), the temperature across the cells is less than in case-2 (2C discharge rate). In both cases, the air mass flow rate is the same but the heat generation in case-2 is around 4 times greater than in case-1 in the cell core. Therefore, in every row of the cell in the battery pack of case-2 (shown in Table 10.2), the temperature is higher as compared to case-1. It is obvious that the surface temperature of cell covers is higher in case-2 as the amount of heat generation is higher in this case. As a result, relatively a higher amount of heat is transferred from cell covers to the air. Hence, the air temperature is also high for case-2.

In both cases (case-1 and 2), it can be visualized that the air temperature increases along the downstream direction. Moreover, the temperature of the cells in the first row is the lowest and it increases consecutively for the cells placed downstream. The air received heat from the first row of cells and its temperature rises. The hot air cannot receive more amount of heat from the next row of cells because the temperature difference between cell cover and air decreases. Hence, the cell temperature placed downstream is higher.

**Fig. 10.2 a** Temperature distribution across the mid-plane of the domain.  
**b** Cell outer surface temperature and velocity contour at the mid-plane, for case-1 and 2



The cell cover surface temperature for case-1 and case-2 is also shown in Fig. 2b. It can be visualized that the temperature of two mid cells in every row has a higher temperature than the side cells. The airflow between the side cells and battery casing receives heat from one side. On another side, it is the battery casing wall. Hence no heat is received from another side. But airflow across the middle cells received heat from both sides. As a result, the air temperature between cells increases. Hence, due to the decrease in temperature difference between mid-cells and air less heat transfer occurs from mid-cells. Therefore, the temperature of two mid cells in every row becomes higher than the side cells.

### 10.3.2 Effect of Air Flow Rate

Figure 10.3a, b, shows the temperature distribution across the mid-plane and surface temperature of cells respectively. In both cases (case-2 and case-3), the discharge rate is maintained at 2C with different air flow rates. From the figures, it has been observed that as the airflow velocity increases, the cell temperature decreases throughout. A huge temperature drop across the cells is observed when the air velocity increases from 0.1 to 0.1 m/s. From Fig. 10.3b, it is observed that the maximum air velocity in the cell gap is around 0.02 m/s for case-2, whereas it is around 0.18 m/s for case-3. When the air velocity increases, the local Reynolds number increases. Hence Nusselt number increases. As a result, the heat transfer coefficient increases with an increase in air velocity. Therefore, the battery cooling is enhanced with an increase in air velocity.

From Fig. 10.4, it is observed that in case-2, the temperature of the cell is highest (363 °C) and it is the lowest for case-3. The highest temperature is obtained at the two mid cells of the last row. In case-2, the 2C discharge rate generates the highest amount of heat while the airflow velocity is maintained at 0.01 m/s. In case-3 it is increased to 10 times. Hence, the cell maximum temperature is the lowest among all the cases.

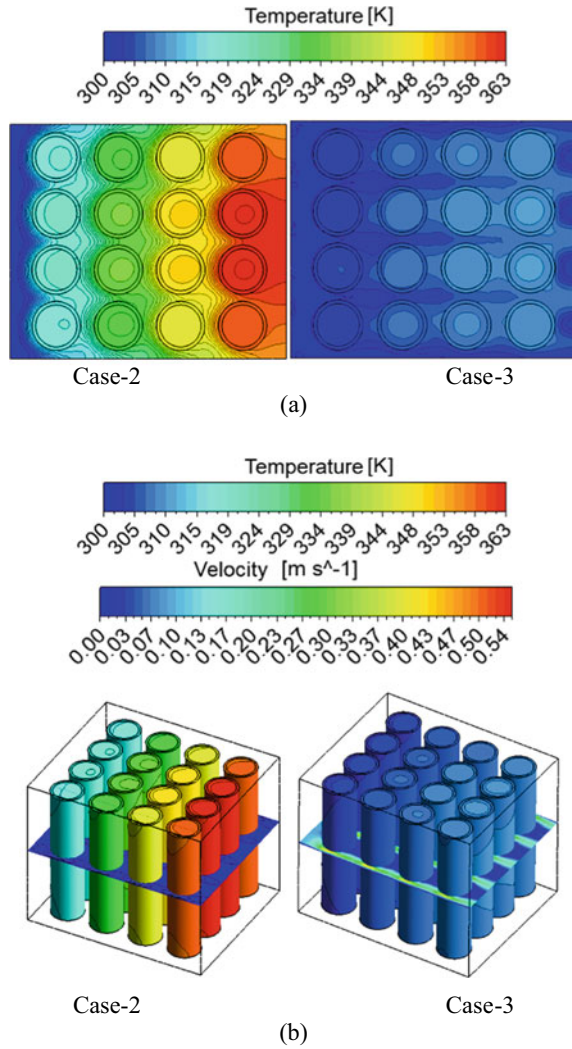
Table 10.3 depicts the amount of heat generated, the amount of heat that enters through inlet air, the total heat energy that moves out from the system, the pressure drop across the battery and the average temperature of outlet air for various cases.

It is observed that in case-1 and case-2, different amount of heat is generated because they have different discharge rate but the airflow velocity is the same. The average temperature of outflow gas is less for case-1 because it has a smaller energy source. However, the pressure drop is the same for case-1 and case-2 because the airflow velocities are the same for both cases. It is observed that in case-2 and case-3 same amount of heat is generated in the cells due to the high discharge rate. In case-3, the heat rejected out is maximum in case-3 due to high airflow velocity and the average temperature of outlet air is 304.87 K. The pressure drop in case-3 is the highest because high flow velocity causes higher frictional losses.

## 10.4 Conclusion

CFD simulations are conducted to determine the cooling of  $4 \times 4$  Lithium-ion battery pack with different discharge rate and with different air flow velocity. The heat generation from cell are determined using the correlation developed by Bernadi. From the result it is observed that with an airflow velocity of 0.01 m/s, when the battery discharge rate is 1C, 2.153 W of heat energy is rejected out from the cells and the average air temperature at the outlet is around 315 K. When the discharge rate increases up to 2C, heat rejection increases to 238% and the temperature of outlet air increases to 13.15%. Similarly, with increase in air flow velocity considering

**Fig. 10.3** **a** Temperature distribution across the mid-plane of the domain. **b** Cell outer surface temperature and velocity contour at the mid-plane, for case-2 and 3



2C discharge rate, the amount of heat rejection increase to 28% and the outlet air temperature decreases to 15%. The pressure drop also increases across the battery pack with increase in airflow velocity.

It is also observed that the last row cells have the highest temperature and the first row cells have the lowest temperature regardless of discharge rate and airflow velocity. The two middle cells of the last row have the highest temperature among all irrespective of discharge and flow conditions. For case-1, case-2 and case-3 the middle cells of the last row have 317 K, 362 K and 310 K respectively.

**Fig. 10.4** Maximum temperature inside the cell

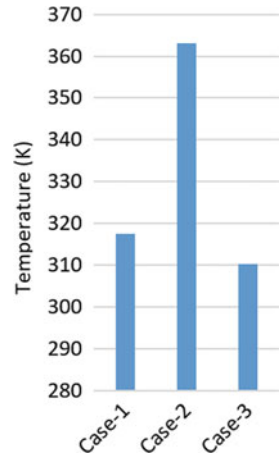


**Table 10.3** Various variables at inlet and outlet for different cases

Case	Flow area (m <sup>2</sup> )	Mass flow rate (kg/s)	Inlet (W)	Energy source (W)	Outlet (W)	Avg. Pressure drop (Pa)	Avg. Temp Outlet (K)
1	0.01	0.0001225	0.2213	1.9323	2.1536	0.0271	315.61
2		0.0001225	0.2213	7.0682	7.2895	0.0271	357.12
3		0.001225	2.2808	7.0682	9.3485	0.4265	304.87

## References

1. Wang, T., et al.: Thermal investigation of lithium-ion battery module with different cell arrangement structures and forced air-cooling strategies. *J. Appl. Energ.* **134**, 229–238 (2014)
2. Wang, T., Tseng, K., Zhao, J.: Development of efficient air-cooling strategies for lithium-ion battery module based on empirical heat source model. *J. Appl. Therm. Eng.* **90**, 521–529 (2015)
3. Saw, L.H., et al.: Computational fluid dynamic and thermal analysis of Lithium-ion battery pack with air cooling. *J. Appl. Energ.* **177**, 783–792 (2016)
4. Xu, X., He, R.: Research on the heat dissipation performance of battery pack based on forced air cooling. *J. Power Sour.* **240**, 33–41 (2013)
5. Jiaqiang, E., et al.: Effects of the different air cooling strategies on cooling performance of a lithium-ion battery module with baffle. *J. Appl. Therm. Eng.* **144**, 231–241 (2018)
6. Tran, T.-H., Harmand, S., Sahut, B.: Experimental investigation on heat pipe cooling for hybrid electric vehicle and electric vehicle lithium-ion battery. *J. Power Sour.* **265**, 262–272 (2014)
7. Wang, Q., et al.: Experimental investigation on EV battery cooling and heating by heat pipes. *J. Appl. Therm. Eng.* **88**, 54–60 (2015)
8. Liang, J., Gan, Y., Li, Y.: Investigation on the thermal performance of a battery thermal management system using heat pipe under different ambient temperatures. *J. Energ. Convers. Manage.* **155**, 1–9 (2018)
9. Chen, F., et al.: Air and PCM cooling for battery thermal management considering battery cycle life. *J. Appl. Therm. Eng.* **173**, 115154 (2020)
10. Verma, A., Shashidhara, S., Rakshit, D.: A comparative study on battery thermal management using phase change material (PCM). *J. Therm. Sci. Eng. Prog.* **11**, 74–83 (2019)



11. Bai, F., et al.: Thermal management performances of PCM/water cooling-plate using for lithium-ion battery module based on non-uniform internal heat source. *J. Appl. Therm. Eng.* **126**, 17–27 (2017)
12. Putra, N., et al.: Performance of beeswax phase change material (PCM) and heat pipe as passive battery cooling system for electric vehicles. *J. Case Stud. Therm. Eng.* **21**, 100655 (2020)
13. Jilte, R., Kumar, R., Ahmadi, M.H.: Cooling performance of nanofluid submerged vs. nanofluid circulated battery thermal management systems. *J. Clean. Prod.* **240**, 118131 (2019)
14. Wiryasart, S., et al.: Thermal management system with nanofluids for electric vehicle battery cooling modules. *J. Case Stud. Therm. Eng.* **18**, 100583 (2020)
15. Huang, Y., et al.: Study on the thermal interaction and heat dissipation of cylindrical lithium-ion battery cells. *J. Energ. Procedia* **142**, 4029–4036 (2017)
16. Bernardi, D., Pawlikowski, E., Newman, J.: A general energy balance for battery systems. *J. Electrochem. Soc.* **132**(1), 5 (1985)